ORIGINAL ARTICLE

Optical Properties of Methyl Orange-Doped Droplet and Photodynamic Therapy of *Staphylococcus aureus*

Soheil Sharifi[1] · Shurshalova Guzel Salavatovna[2] · Afshin Azarpour[1] · Forough Rakhshanizadeh[3] · Gholamhossein Zohuri[4] · Mohammad Reza Sharifmoghadam[5]

Abstract

Dye-doped droplets are known as mixtures of dyes with uniform solutions of water droplets in a continuous phase of oils with surfactants. To observe the relationship between water droplet structures and surfactant types on optical properties of dyes, a mixture of methyl orange (MO)-doped droplet prepared with benzene and hexane as oils and sodium bis(2-ethylhexyl) sulfosuccinate (AOT) as a surfactant was thus examined using Z-scan instrument, spectrophotometer, and fluorimeter in the present study. The findings revealed that nonlinear refractive (NLR) index, nonlinear absorption (NLA) coefficient, as well as fluorescence intensity of the MO had enhanced following a reduction in the droplet water content induced by changes in the non-centrosymmetric charge density distribution of this pH indicator. Moreover, the MO-doped droplet in a continuous phase of benzene investigated by ^{1}H nuclear magnetic resonance (NMR) spectroscopy indicated that the MO had been located in the droplet in the vicinity of the hydrophilic part of the surfactant. Furthermore, the MO-doped droplets along with laser radiation were employed to perform antibacterial photodynamic therapy (APDT) of *Staphylococcus aureus* (*S. aureus*). It was ultimately concluded that the bacteria colony had also extremely diminished in the group treated by the MO-doped droplet.

Keywords Methyl Orange · Surfactant · Photodynamic therapy · *Staphylococcus aureus*

Introduction

Characterized by huge optical nonlinearity, nonlinear optical (NLO) materials can have applications in antibacterial photodynamic therapy (APDT) [1–3]. In this respect, enhancement of nonlinearity of materials has been assumed as one of the interesting topics with several applications. The NLO properties of materials can also change due to environmental effects such as cis-trans transition [4], phase transition [5], as well as solvent polarity [6, 7]. Besides, some techniques are available to find the NLO values of dyes; e.g. four-wave mixing and Z-scan technique. In this regard, the Z-scan technique has been recognized as a high-sensitivity and simple method to examine third-order NLO parameters such as nonlinear refractive (NLR) index and nonlinear absorption (NLA) coefficient [8].

The Z-scan technique, presented by Sheik-Bahae, was created on a laser beam and distributed via an NLO material [9]. Accordingly, several studies have been conducted on NLO properties of organic dyes [10, 11]. Most of these investigations have been performed on azo and xanthene dyes with regard to their applications in medicine and biological phenomena [12, 13]. Methyl orange (MO), as a pH indicator, has been correspondingly utilized in the form of a probe for carrying out experiments on interactions in proteins [14] and surfactants [15]. In previous studies, the NLR index and the NLA coefficient of MO have been further investigated via Z-scan technique under different pH conditions [16], demonstrating that cis-trans transition is able to change the NLO properties of MO. The findings have also suggested that

✉ Soheil Sharifi
  ssharifi@ferdowsi.um.ac.ir; soheil.sharifi@gmail.com

1 Department of Physics, Faculty of Science, Ferdowsi University of Mashhad, Mashhad, Iran

2 Kazan (Volga Region) Federal University, 18 Kremlevskaya St., Kazan, Russian Federation 420008

3 Department of Pediatrics, Faculty of Medicine, Mashhad University of Medical Sciences, Mashhad, Iran

4 Department of Chemistry, Faculty of Science, Ferdowsi University of Mashhad, PO Box 91775, Mashhad, Iran

5 Department of Biology, Faculty of Sciences, Ferdowsi University of Mashhad, Mashhad, Iran

azobenzene polymer can strongly influence optical responses of MO [17].

To the best of authors' knowledge, the NLO properties of MO in droplets and microemulsions (MEs) as optical transparent mixtures and uniform solutions of oil, water, and surfactants in which water droplet can be combined with dyes had not been already published [18]. The MEs can also have water-in-oil (W/O) phase in which water and surfactants can produce a nano-droplet in a continuous phase of oil. In the mixture of hydrophilic dye with a nano-droplet, the dye can similarly stay inside a water droplet and the position of the dye in the droplet can control the NLO properties. The nano-materials have a lot of application in antimicrobial, sensing biomaterials and cancer tretment, [19–21].

The APDT has been introduced as a method to kill bacteria via oxidation in a precise manner [22]. Within the APDT, singlet oxygen can be thus produced through an interaction between laser light and photosensitizers and consequently destroy bacteria [23]. One method to enhance singlet oxygen can be an increase in NLA in mediums. In this respect, it has been reported that singlet oxygen can be generated through two-photon excitation [24, 25]. For example, the APDT of *S. aureus* had been investigated in a previous study using hydrogel prepared with peptide-modulated self-assembly of fullerenes [26].

In the present study, linear and NLO properties of MO-doped nano-droplet were thus reported and compared with surfactant effects. The main objective of this study was to examine the effect of the droplet size in a nanometer scale on the NLO of the MO. Accordingly, it was observed that the NLA of the MO-doped droplet had been enhanced compared with the MO from aqueous solution. The ^{1}H nuclear magnetic resonance (NMR) spectroscopy was also utilized to determine the position of the MO inside the droplet. The APDT of *S. aureus* was further assessed using the MO in the ME as a photosensitizer and laser radiation to produce the NLA. Ultimately, it was investigated whether the MO-doped droplet could be used for the APDT of *S. aureus*.
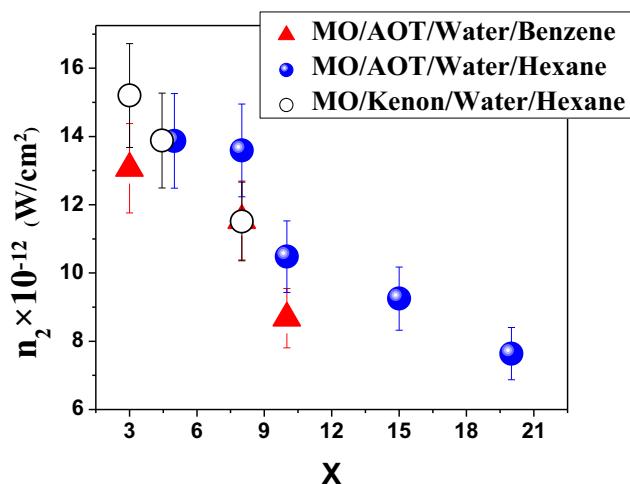

Fig. 2 The n_2 values of MO/AOT/Water/Hexane (Close Circles), MO/Kenon/Water/Hexane (Open Circles) and MO/AOT/Water/Benzene (Open up-triangles) as a function of molar ratio(X) at a constant MO concentration (C_{MO} = 0.0285 mM)

Experiment

Materials and Preparation

MO, sodium bis(2-ethylhexyl) sulfosuccinate (AOT), cetyltrimethylammonium bromide (CTAB), dimethylformamide (DMF), methanol, ethanol, i-propanol, hexane, and benzene were purchased from Sigma-Aldrich Corporation. Two types of solutions were arranged to examine NLO properties: (1) a mixture of MO in water (MO-H$_2$O) and MO in ME (MO-ME). Accordingly, the microemulsion was prepared by a mixture of water, oil (hexane and benzene), and surfactant (AOT) in which the ratio of water-to-surfactant molar ratio was defined by X = [H$_2$O]/[AOT] and droplet concentration was described by droplet mass fraction $\{m_{fd} = (m_{H2O} + m_{AOT})/(m_{Total})\}$, wherein m_{Total} is mass of water, surfactant, and oil in the ME. It should be noted that the ME was prepared at different water-to-AOT molar ratios (between 3 to 20). The concentration of dye in ME was also explained by weight in terms of mass of MO in ME (C_{MO});
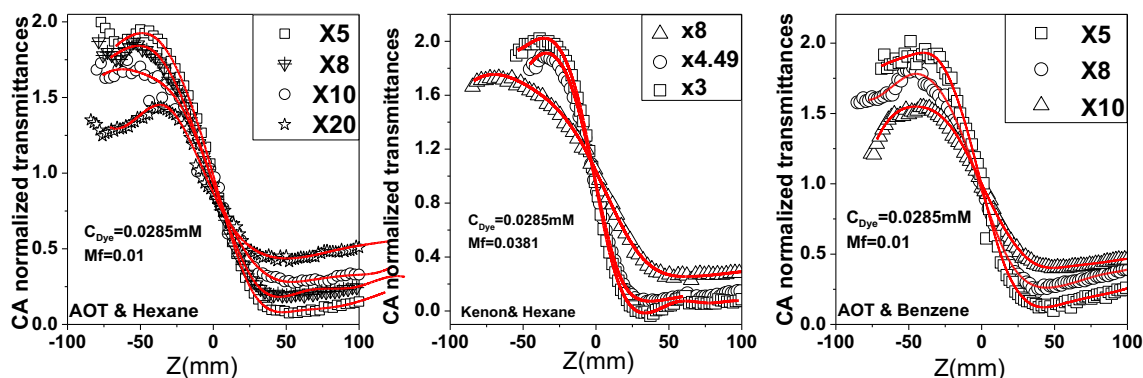

Fig. 1 The close aperture curves of (**a**) MO/AOT/Water/Hexane (C_{dye} = 0.0285 mM - mf = 0.01) and **b** Methyl Orange/Kenon/Water/Hexane at (C_{dye} = 0.0285 mM - mf = 0.0381) and (c) Methyl Orange/AOT/Water/Benzene (C_{dye} = 0.0285 mM - mf = 0.01) at different molar ratio (X)

(2) a mixture of aqueous solutions of MO with AOT and Kenon. The absorption and fluorescence spectra of MO in different solutions (methanol, ethanol, i-propanol, and water) and ME were investigated.

According to CLSI protocol, a pure bacterial culture of a standard bacillus strain, was suspended in a buffer, standardized to turbidity and swabbed uniformly across a culture plate, and incubated for 16–24 h at 37 °C.

Instruments

In this study, a Gaussian beam with a continuous-wave (CW) laser ($\lambda = 532$ nm, with 80 mW) was used in the Z-scan technique. The laser beam was focused by a 5.0 cm lens. The beam radius (ω_0) and Rayleigh length (z_0) were also reported by 1.4 μm and 1.1 mm; respectively. Absorbance and fluorescence spectra of the samples were then recorded using UV-1650 PC spectrometer (Labomed Inc.) and FP-6200 spectro-fluorometer (Jasco Inc.).

All ^{1}H NMR experiments were performed on a Bruker Avance II 500 ^{1}H NMR spectrometer equipped with a 5-mm probe using the standard Bruker TopSpin Software. Temperature control was also fulfilled using a Bruker variable temperature unit (BVT-3000) in combination with a Bruker cooling unit (BCU-05). The experiments were conducted at 303 K without sample spinning. Chemical shifts were then given in values of parts per million, referenced to residual solvent signals (7.16 ppm for residual ^{1}H in C6D6). ^{1}H NMR data were similarly collected with 32 k complex data points. Moreover, 1D ROESY experiments were carried out using pulse sequences, described in Refs. [27, 28]. Gaussian-shaped pulses were correspondingly used for radio frequency irradiation. The repetition time between subsequent runs of the rotating frame overhauls effect spectroscopy (ROESY) sequence was also reported at least three times longer than the mean proton T1 for the molecules. Furthermore, mixing time elevated from 0.05 to 0.5 s. In this respect, inversion-recovery experiments were performed using the Bruker T1IR pulse program, using standard acquisition parameters. T1 values were then calculated using the T1 relaxation routine (Topspin 2.1), [29, 30].

Results and Discussion

NLO Properties of MO

The close aperture curves of the MO/AOT/water/hexane, the MO/kenon/water/hexane, and the MO/AOT/water/benzene at different molar ratios (X) and with constant MO concentrations ($C_{MO} = 0.0285$ mM) are illustrated in

Fig. 1a, b,c. The difference between the maximum and the minimum of the closed aperture is given in the following equation [31]:

$$\Delta T_{P-V} = 0.406(1-S)^{0.25}\Delta\Phi_0 \qquad (1)$$

here; $\Delta\Phi_0$ refers to phase distortion and S represents aperture transmittance [32, 33]. The n_2 can be also calculated from ΔT_{p-v} using Eq. 2:

$$n_2 = \left(\lambda\Delta T.\Delta T_{P-V} = 0.406(1-S)^{0.25}\Delta\Phi_0 - S)^{0.25}\right) \qquad (2)$$

The n_2 as the function of molar ratio (X) is displayed in Fig. 2. The value of n_2 had thus reduced following the rise in X (droplet size). The closed aperture curves
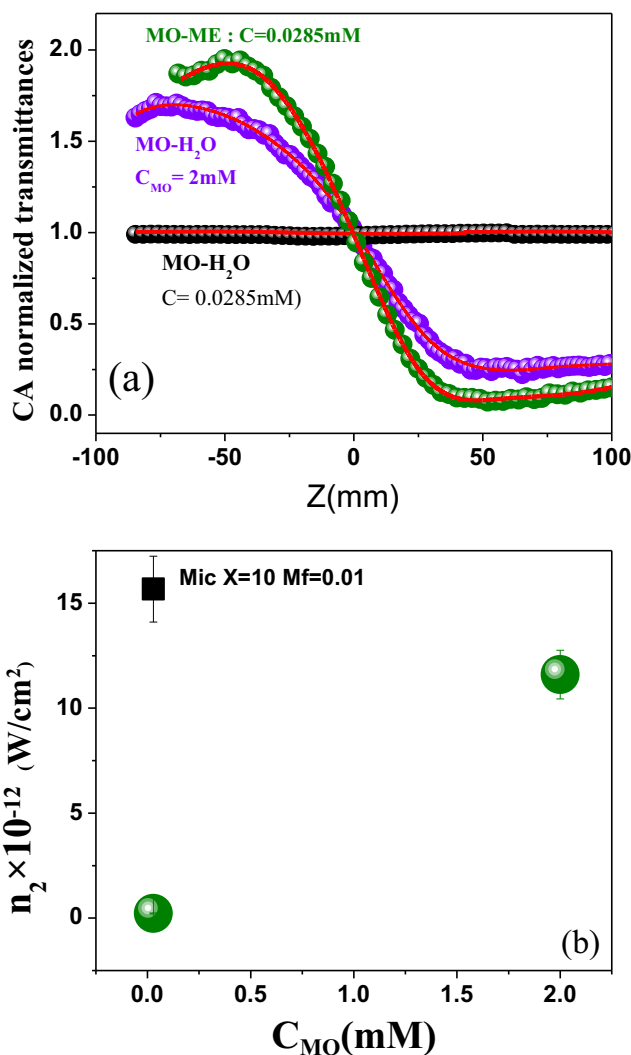

Fig. 3 **a** The close aperture curves of MO/AOT/Water/Hexane at mf = 0.01, X = 10 and C_{dye} = 0.0285 mM and MO-H_2O at two MO concentration (C_{dye} = 0.0285 mM and 2 mM). **b** The n_2 values of MO-ME (Cubic) and MO-H_2O (Close circle)
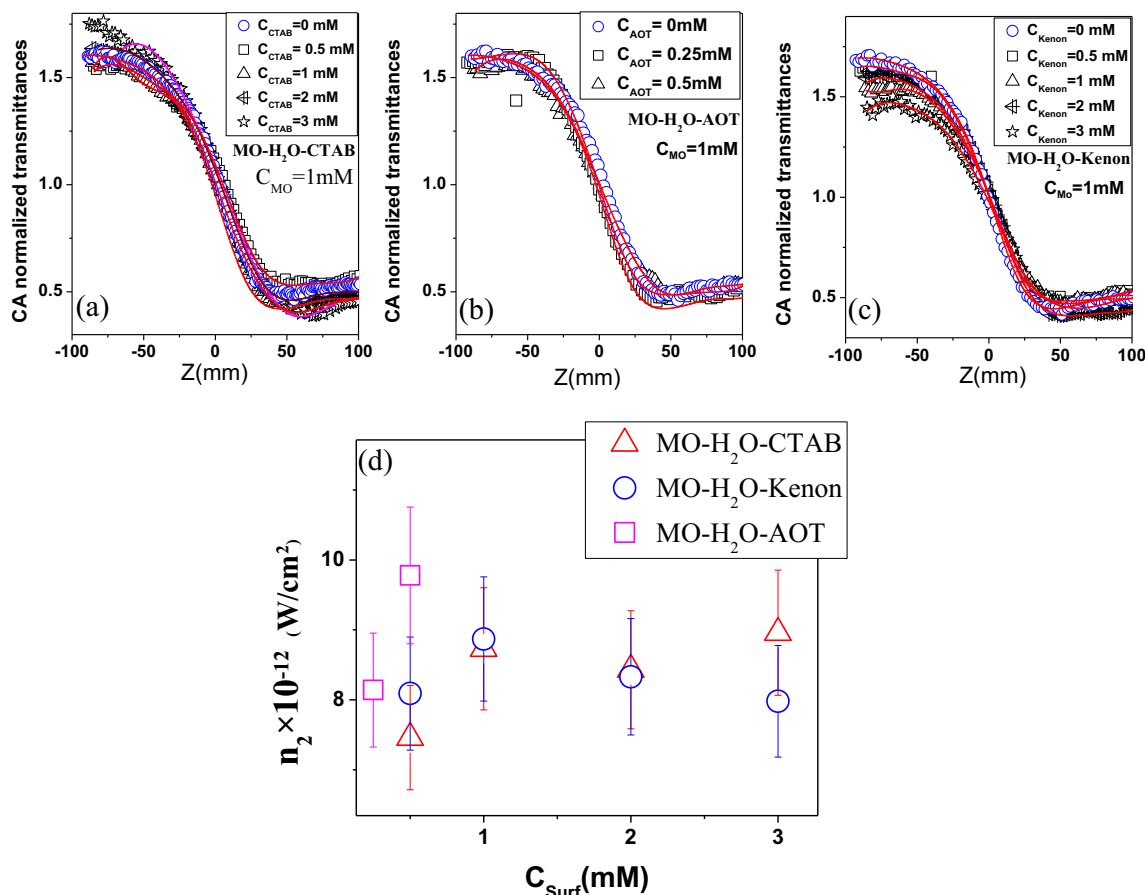
Fig. 4 The close aperture curves of MO-H$_2$O (C$_{MO}$ = 1 mM) with different concentration of (**a**) CTAB, **b** AOT and **c** Kenon. **d** The n$_2$ values as a function of surfactant concentration of CTAB (Up-triangle), AOT (Cubic) and Kenon(Circle)

of the MO-ME and the MO-H$_2$O (C$_{MO}$ = 0.0285 mM) were further studied, whose results are presented in Fig. 3 (a). According to Fig. 3b, the n$_2$ value of the MO-ME is higher than that of the MO-H$_2$O at C$_{MO}$ = 0.0285 mM; due to the polarity of the solution, since the polarity of the ME is less than water. Moreover, the thermo-optic coefficient of the materials could be obtained from the n$_2$ value via Eq. 3 [34]:

$$n_{2thermal} = \left(\frac{dn}{dt}\right) \alpha\omega_0^2 \Big/ 4k \qquad (3)$$

Table 1 The nonlinear refractive index (n$_2$), third-order susceptibility (χ_R) and second-order hyperpolarizabilities (γ_R) of MO-ME

Sample	C$_{MO}$ (mM)	mf	X	n$_2$(10^{-12}m^{2}W^{-1})	$\chi_R^{(3)}$(m^3 W^{-1} s^{-1})	γ_R(10^{-25}m^{6}W^{-1} s^{-1})
MO/AOT/Water/Benzene	0.0285	0.01	10	4.60785	0.0321	4.62988
			8	7.20749	0.05021	7.24195
			3	9.91867	0.06909	9.9661
MO/AOT/Water/Hexane	0.0285	0.01	5	13.87	0.05561	11.4541
			8	13.59	0.05449	11.2229
			10	10.48	0.04202	8.65457
			20	7.638	0.03062	6.3076
MO/Kenon/Water/Hexane	0.0285	0.0381	3	15.2	0.06094	2.73087
			4.449	13.88	0.05565	2.49372
			8	11.51	0.04615	2.06792

Table 2 The n_2, χ_R and γ_R of MO/AOT/Water/Hexane and MO-H_2O

Sample	C_{MO}(mM)	$n_2(10^{-12}m^2W^{-1})$	$\chi_R^{(3)}(m^3\ W^{-1}\ s^{-1})$	$\gamma_R(10^{-23}m^6W^{-1}\ s^{-1})$
Mic Mf = 0.01 X10	0.0285	15.67	0.06283	0.129405
Water	0.0285	0.22	1.50487	3.49021
	2	11.6	79.34774	2.62242

wherein, α, k, and dn/dt show absorption coefficient, thermal conductivity, and thermo-optic coefficient; respectively. It should be noted that an increase in the n_2 value together with a reduction of the droplet size can be due to changes in the dn/dt. However, reduction in the n_2 value in the MO-H_2O can be induced by thermal conductivity, since the thermal conductivity of water is higher than ME.

The effect of cetrimonium bromide (CTAB), AOT, and kenon concentrations on the n_2 values in the MO-H_2O

Fig. 5 a The open aperture curves of MO/AOT/Water/Hexane at mf = 0.01, X = 10 and C_{MO} = 0.3 mM and MO-H_2O at C_{MO} = 0.3, 12, 15 mM. **b** The β values as function of MO concentration at MO-ME (Cubic) and MO-H_2O (Circles)

solutions were also examined as illustrated in Fig. 4a, b, c. Accordingly, the n_2 values did not change following variations in cationic (CTAB), anionic (AOT), and nonionic (kenon) surfactant concentrations in the solution (Fig. 4d). Thus, the surfactant type and concentrations could not change the dn/dt values. Therefore, the change in the n_2 value in the MO-ME with the droplet size could not come from the interaction between the MO and the AOT.

Third-order susceptibility (real part) was also related to the n_2 and it could be evaluated by Eq. 4 [35]:

$$\chi_R^{(3)} = 2n_2n_0^2\varepsilon_0^2c \qquad (4)$$

wherein, n_0 and c indicate refractive index and light velocity; respectively. In the real part of second-order hyperpolarizabilities, γ_R is also represented by Eq. 5 [36].

$$\gamma_R = \frac{\chi_R^{(3)}}{L^4N} \qquad (5)$$

in which, L stands for Lorenz correction factor. The χ_R and γ_R values of the MO-ME are presented in Table 1 and the χ_R and γ_R values of MO/AOT/water/hexane and MO-H_2O are listed in Table 2. According to the results, the γ_R values of the MO-ME were very smaller than those of the MO-H_2O and they reduced following the increase in the X. It is also known that the second-order NLO is due to a growth in non-centrosymmetric charge density distribution. Thus, the NLO properties of the MO could change based on the droplet size due to charge density distribution. In an earlier study, sulphide glass-containing b-GeS2 microcrystallites had been also examined and it had been reported that the NLO properties had been influenced by electron-phonon sub-systems [37]. It had been further suggested that non-centrosymmetric charge density distribution could affect second-order NLO properties [38, 39]. A theoretical study had been also conducted using ultraviolet-visible (UV) spectroscopy of 6-substituted benzodifuran derivatives [40]. In this respect, second-order hyperpolarizability could depend on the length of the π-conjugated way and the force on donor-acceptor substituents. The origin of second-order hyperpolarizability could be also related to non-cetrosymmetry in charge density distribution. Thus, NLO properties of MO could be changed by molecule charge density distribution or be subject to molecular dipole moment.
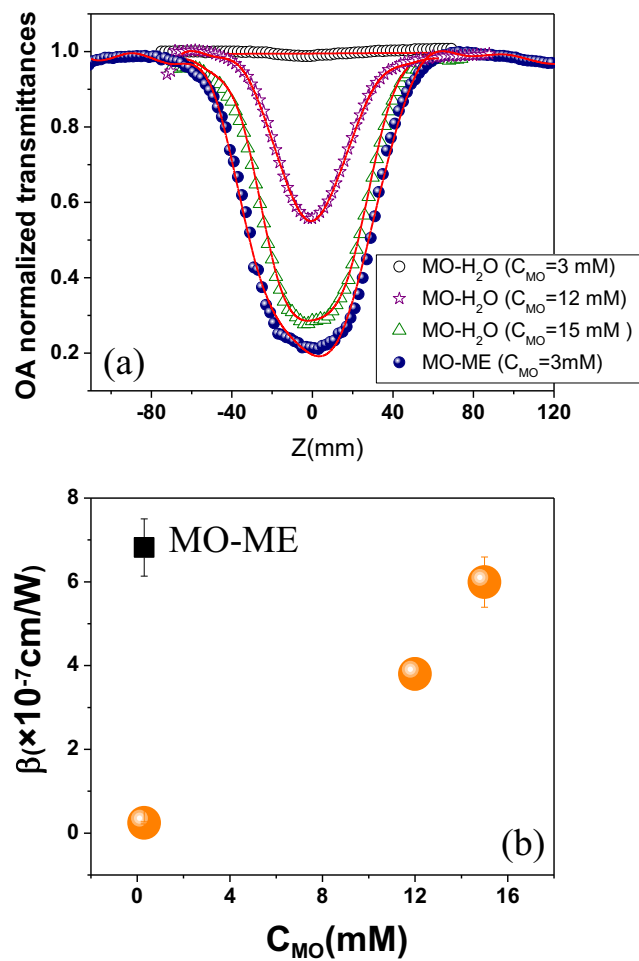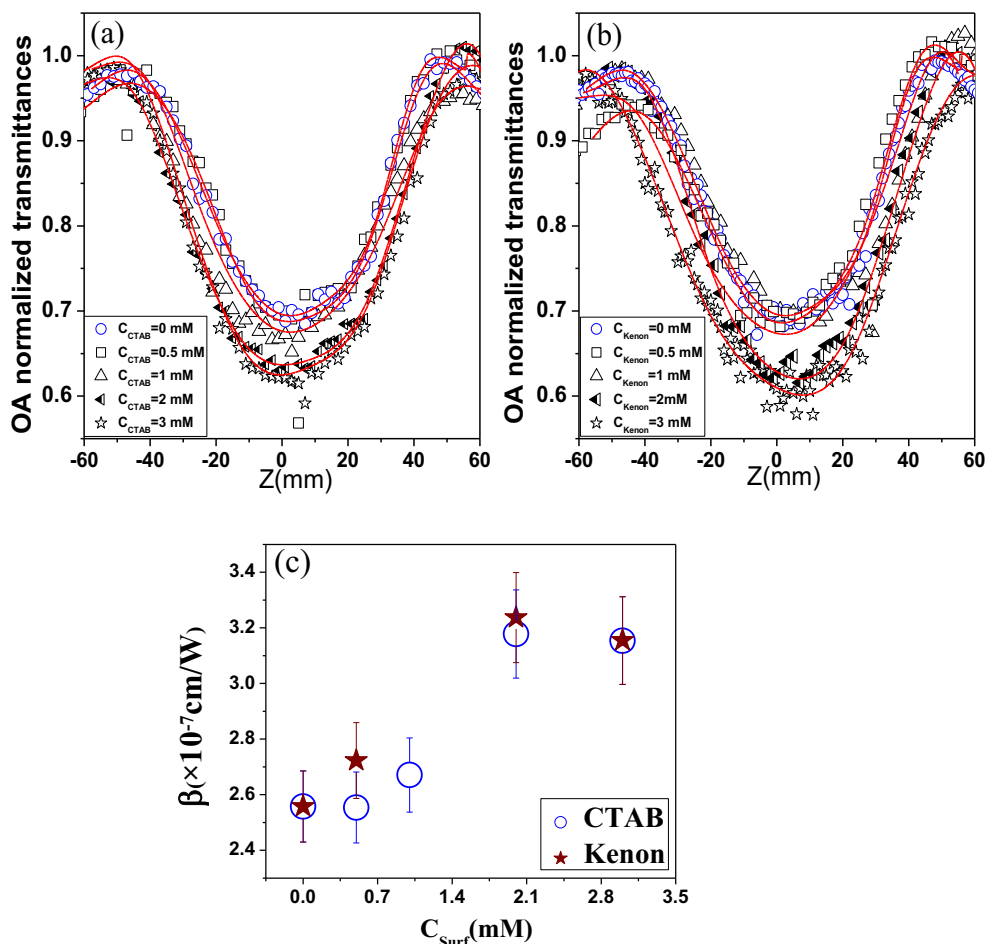
Fig. 6 The open aperture curves of MO-H2O at constant MO concentration ($C_{MO} = 15$ mM) with different concentration of **a** CTAB, **b** Kenon. **c** The β values as a function of surfactant concentration of CTAB (Circle) and Kenon (Stars)


Moreover, second-order hyperpolarizability of 4-octadecyl-4′-nitrostilbene (OANS) in Langmuir-Blodgett (L-B) films had been examined in previous studies [41], suggesting that OANS aggregation in L-B films could enhance second-order hyperpolarizability of OANS. In the present

case, the ME could reduce dye aggregation compared with aqueous solutions and it could correspondingly mitigate second-order hyperpolarizability of the MO-ME.

The open aperture curves of the MO-ME and the MO-H$_2$O are shown in Fig. 5a. Accordingly, the results revealed that the

Fig. 7 a Fluorescence spectra (**b**) absorbance of MO in solvent and microemulsion
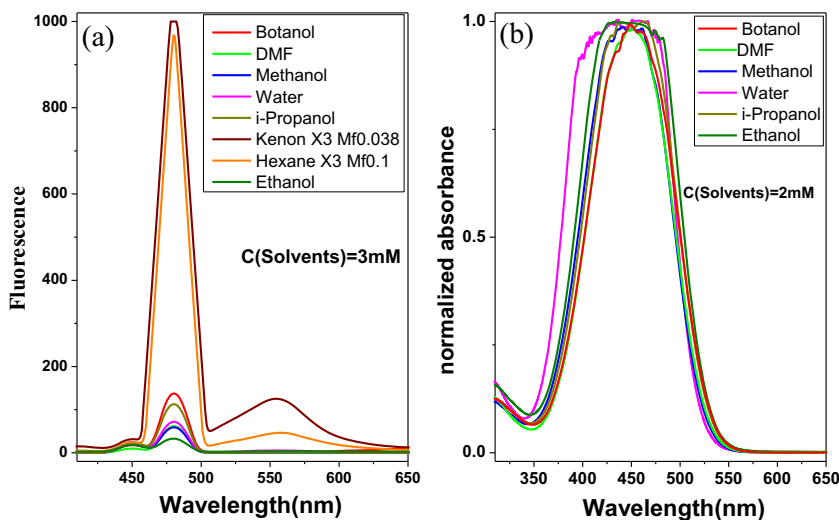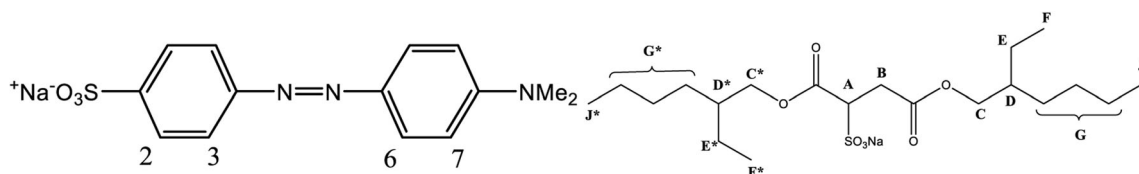
Fig. 8 Chemical structure of methyl orange (left) and AOT (right)

MO-ME (X = 10, mf = 0.1, C_{MO} = 0.3 mM) had a minimum at Z = 0, while the open aperture curves of the MO-H_2O (C_{MO} = 0.3 mM) showed a straight line. The NLA was correspondingly found from an open aperture curve, fitted by Eqs. 6 and 7 [42].

$$q_0 = \beta I_0 L_{eff} \left(1 + \left(\frac{Z}{Z_0} \right)^2 \right)^{-1} \tag{6}$$

That q_0 is:

$$T_{OA} = \sum_{x=0} (-q_0)^x (x+1)^{-1.5} \tag{7}$$

where, L_{eff} and z_0 represent effective thickness and Rayleigh length; respectively. As well, I_0 refers to laser intensity of focus and β shows NLA coefficient. The β value was also extracted from Eqs. 6 and 7. According to Fig. 5b, the β value of the MO-ME was higher than that of the MO-H_2O at C_{MO} = 0.3 mM. Moreover, the β value of the MO-H_2O enhanced following an increase in MO concentration, from 3 to 15 mM. In Fig. 5, the open aperture curves could be related to reverse saturable absorption (RSA) which depended on two-photon absorption (TPA) and excited state absorption (ESA). It should be noted that the MO had a peak absorbance at 450 nm [43] and a weak one at 532 nm; indicating TPA. Thus, the TPA of the MO-ME enhanced compared with aqueous solution, probably due to reduction of medium polarity in the ME.

In this study, the open aperture curves of the MO-H2O at different CTAB and kenon concentrations are presented in Fig. 6a, b.
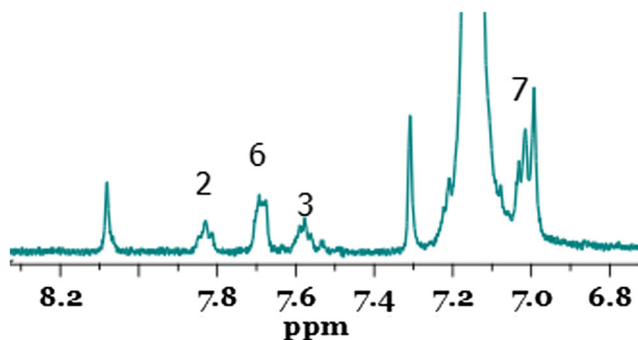
The results showed that the depth of the open aperture curves had increased following a growth in surfactant concentration in solutions, thus the β value increased from 2.5×10^{-7} to 3.1×10^{-7} cm/W with a rise in surfactant concentration from 0 to 3 mM (Fig. 6c). The increase in the value of β with a rise in the surfactant concentration might be due to the growth in MO solubility. Typically, a micelle in aqueous solution is produced with an aggregate of the hydrophobic tail of surfactant. The number of micelles can thus increase following a rise in surfactant concentration in aqueous solutions and more micelles can enhance dye solubility in solution. Therefore, the NLO properties can be boosted following an increase in MO solubility.

To improve the results, fluorescence and absorbance spectra of the MO in different solvents were studied whose results are presented in Fig. 7a, b; indicating that the peak position of fluorescence and absorption spectra did not depend on the polarity of mediums. However, the fluorescence spectra enhanced in the MO-ME due to increased lifetime of the excited level following the growth in NLA coefficient.

^{1}H NMR Spectrum of MO in AOT/Water/Benzene

The ^{1}H NMR spectrum of the MO in the AOT/water/benzene (Fig. 8) solution is shown in Fig. 2. Signals on the spectra
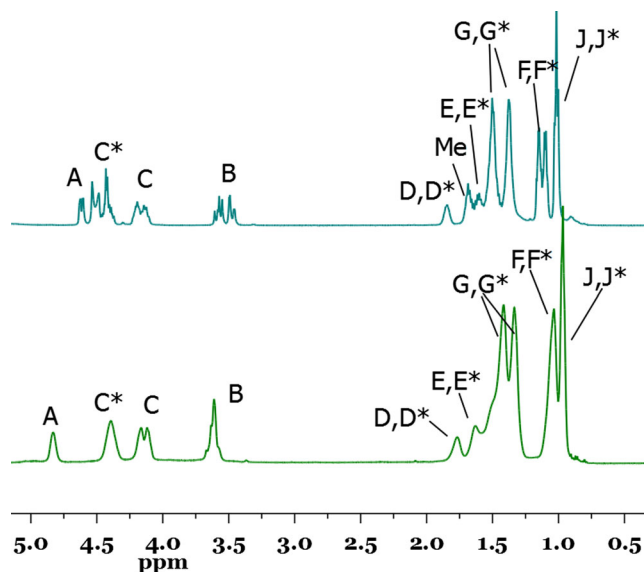

Fig. 9 ^{1}H NMR spectrum of methyl orange in AOT/Water/Benzene, T = 303 K. Methyl orange signals are marked by arabic numbers

Fig. 10 ^{1}H NMR spectrum of MO/AOT/Water/Benzene (upper) and ^{1}H NMR spectrum of AOT/Water/Benzene (bottom). T = 303 K. AOT signals are marked by latin letters
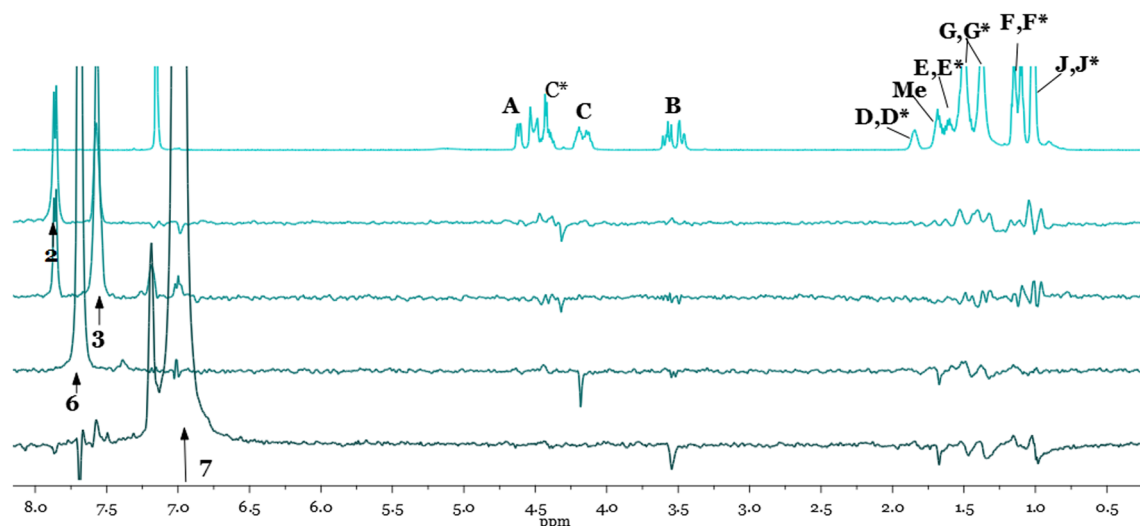
Fig. 11 ^{1}H NMR spectrum of MO/AOT/Water/Benzene (upper) and 1D selective ROESY NMR spectra of MO/AOT/Water/Benzene, T = 303 K, mixing time 0.3 s. The arrows indicate the signals with the frequency of applied selective RF pulses

were thus assigned according to the data in the related literature [44]. This spectrum contained weak peaks of MO in the aromatic region from 7 to 8 ppm. The MO signals were also indicated by Arabic numbers (Fig. 9).

The ^{1}H NMR spectrum of the AOT in the presence and absence of the MO was illustrated in the bottom, containing strong signals of sodium docusate signed by capital Latin letters [45]. The ^{1}H NMR signals of the AOT were also different in pure benzene solution and in those with MO dye (Fig. 3). Proton signals of the micelle model (A, B) in the ^{1}H NMR spectrum also exhibited a strong high field shift. Moreover, it was observed that the signal shape had changed the spectrum in the presence of the dye (Fig. 10) for A, B, C*, and F protons. Such differences in the spectra indicated that the MO had probably formed a molecular complex with the AOT reverse micelle. Reverse micelles one-dimensional (1D) selective rotating-frame overhauser spectroscopy (ROESY) experiments were additionally carried out in order to investigate the interaction between azophloxine dye and docusate sodium. It should be noted that such experiments are based on a measurement of nuclear overhauser effect (NOE) in a rotating frame. The NOE has been also recognized as a powerful tool to determine molecular spatial structure as well as structure of molecular complexes, particularly those with micelles [46–48]. It has been stated that; after excitation of the sample with a radio frequency field (RF field) via a frequency corresponding to the desired signal in the 1D selective ROESY experiment, only those signals can arise in the spectrum whose nuclei are closer to the excited one (distance<5 Å) [28]. The 1D selective ROESY spectra of the MO/AOT/water/benzene obtained after excitation of the sample on the frequencies of CH-2, CH-3, CH-6, and CH-7 signals of the MO are illustrated in Fig. 11.

There were also numerous NOEs between aromatic protons of the MO and almost all protons of docusate sodium on the ^{1}H selective ROESY spectrum (Fig. 11). Accordingly, this assumption was confirmed that the dye could probably intercalate in the reverse micelles in the AOT/water/benzene solution. The most intensive peaks similarly corresponded to the exterior part of the micelle. Thus, it was concluded that the MO had been located in the external part of the micelle, most of the time, near to hydrophilic tails of docusate sodium. However, large numbers of the observed NOEs implied high mobility of the MO molecule in the micelle.

According to the results, the MO stayed in the vicinity of the hydrophilic of the surfactant and it could interact with their head group. Thus, interactions between the dye and the surfactant could change the NLA and consequently enhance the fluorescence spectra of the MO.

In Vitro APDT of *S. aureus*

Based on the study results, the NLA value of the MO-ME was higher than that of the MO-H$_2$O; thus, the MO/AOT/water/hexane could be suggested as a useful material for APDT. In this study, the APDT of *S. aureus* was examined via clonogenic assay, as presented in Fig. 12. The samples of the bacteria with the MO-ME are also illustrated in Fig. 12a and the bacteria and the MO-ME with laser irradiation are shown in Fig. 12b. Accordingly, the findings revealed that the bacteria colony had extremely reduced in the group treated with the mixture of the MO-ME with light irradiation. Moreover, the bacteria colony was studied in the petri with the MO-H$_2$O, as depicted in Fig. 12c, d; and the results were then compared with reference to petri (Fig. 12e). Ultimately, the results demonstrated that the bacteria colony in the samples with the MO-

Fig. 12 The *S. aureus* with (**a**) MO-ME without laser irradiation (**b**) MO-ME under laser irradiation. The *S. aureus* with (**c**) MO-H$_2$O without laser irradiation, **d** MO-H$_2$O under laser irradiation and (**d**) reference ptri
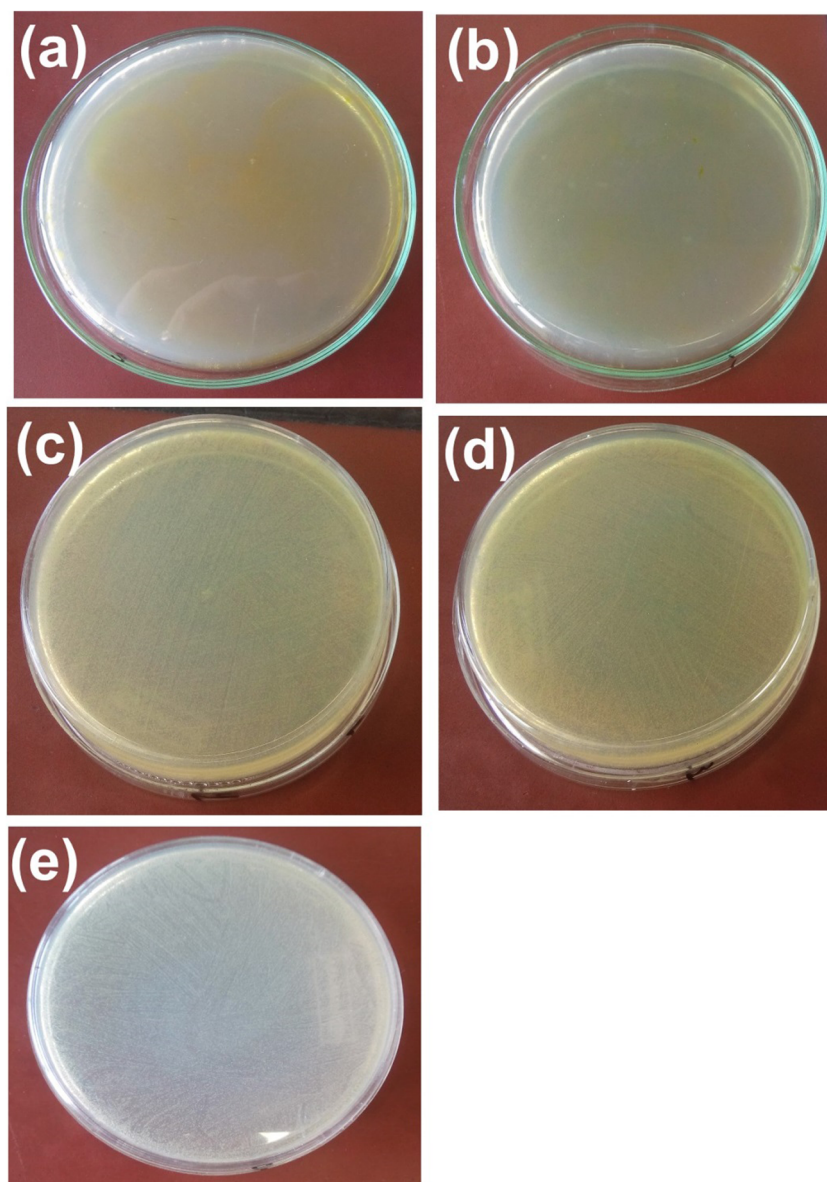
H$_2$O was higher than those with the MO-ME. Thus, the MO-ME was recommended as a good photosensitizer for the APDT of *S. aureus*.

Conclusion

The effect of droplet, water content of AOT/water/hexane, AOT/water/benzene, and kenon/water/hexane on NLP properties of MO using Z-scan technique were investigated in this study. The findings revealed that the NLA coefficient and the NLR index of the MO had reduced following an increase in the water content of the droplet. Thus, the behavior of the MO became similar to water as the water content of the droplet elevated. The type of surfactant did not also change the NLO properties of the MO, while it could vary based on bulk polarity. The value of the second-order hyperpolarizibility, i.e. γ_R, of the MO in water additionally enhanced compared with ME due to changes in non-centrosymmetric charge density distribution of the MO. The medium polarity and the structure of the droplet could correspondingly charge density distribution of the MO. Moreover, the reverse saturable absorption was observed in the MO in the ME consisting of two-photon absorption. The NLA of the MO in the ME was thus reported to be extremely higher than water and it could be of use for APDT. Therefore, the MO-doped droplet could be recommended for the APDT of *S. aureus* since a reduction in bacteria colony was observed under treatments.

References

1. Kachynski AV, Pliss A, Kuzmin AN, Ohulchanskyy TY, Baev A, Qu J, Prasad PN (2014) Photodynamic therapy by in situ nonlinear photon conversion. Nat Photonics 8:455–461

2. Zhou X, Chen Y, Su J, Tian X, Luo Y, Luo L (2017) In situsecond-harmonic generation mediatedphotodynamic therapy by micelles co-encapsulating coordination nanoparticle and photosensitizer. RSC Adv 7:52125–52132

3. Chandra Ray P (2010) Size and shape dependent second order nonlinear optical properties of Nanomaterials and its application in biological and chemical sensing. Chem Rev 110(9):5332–5365

4. Turton David A, Martin David F, Wynne K (2010) Optical Kerr-effect study of trans- and cis-1,2-dichloroethene: liquid–liquid transition or super-Arrhenius relaxation. Phys Chem Chem Phys 12:4191–4200

5. Vogt H (1974) Study of structural phase transitions by techniques of nonlinear optics. Applied Physics A 5(2):85–96

6. Azarpour A, Sharifi S, Rakhshanizadeh F (2018) Nonlinear optical properties of Crocin: from bulk solvent to nano-confined droplet. J Mol Liq 252:279–288

7. Hoseini M, Sazgarnia A, Sharifi S (2019) Cell culture medium and nano-confined water on nonlinear optical properties of Congo red. Opt Quant Electron 51:144–121. https://doi.org/10.1007/s11082-019-1865-1

8. Al-Ahmad AY, Shabeeb Gh M, Abdullah AQ, Ziadan KM (2011) Z-scan measurement for the nonlinear absorption and the nonlinear refraction of poly1,4-diazophenylene-bridged-tris(8-hydroxy-quinoline) aluminum (PDPAlq3). Optik 122(21):1885–1889

9. Sheik-Bahae M, Said AA, Wei TH, Hagan DJ, Stryland EV (1990) Sensitive measurement of optical nonlinearities using a single beam. IEEE J Quantum Electron 26(4):760–769

10. Choubey RK, Medhekar S, Kumar R, Mukherjee S, Kumar S (2014) Study of nonlinear optical properties of organic dye by Z-scan technique using He–Ne laser. J Mater Sci: Mater Electron 25(3):1410–1415

11. Mousavi Z, Ghafary B, MajlesAra MH (2019) Fifth- and third-order nonlinear optical responses of olive oil blended with natural turmeric dye using z-scan technique. J Mol Liq 285:444–450

12. Tingchao H, Changshun W (2008) Study on the nonlinear optical properties of three azo dyes by Z-scan measurements. J Mod Opt 55(18):3013–3020

13. Sangsefedi AS, Sharifi S, Rezaion HRM, Azarpour A (2018) Fluorescence and nonlinear optical properties of alizarin red S in solvents and droplet. J Fluoresc 28(3):815–825

14. Singh SP, Rathinam K, Kasher R, Arnusch Ch J (2018) Hexavalent chromium ion and methyl orange dye uptake via a silk protein sericin–chitosan conjugate. RSC Adv 8:27027–27036

15. Dutta R, Bhat SN (1993) Interaction of methyl Orange with Submicellar cationic surfactants. Bull Chem Soc Jpn 66(9):2457–2460

16. Del Nero J, de Araujo RE, Gomes AS, de Melo CP (2005) Theoretical and experimental investigation of the second hyperpolarizabilities of methyl orange. J Chem Phys 122(10):104506

17. Yi Z, Zhi-Hua P, Fu-Li Z, Mu Q, Yan Z, Chang-Shun W (2014) Nonlinear optical properties of an azobenzene polymer. Chin Phys B 23(2):024212

18. Sharifi S, Jensen GV, Pedersen JS, Marti O, Amirkhani M (2013) The mixture of poly(propylene-glycol)-block-poly(ethylene-glycol)-block-PPG with C12E5 microemulsion. Phys Chem Lliq 51(4):469–479

19. Khatami M, Varma RS, Zafarnia N, Yaghoobi H, Sarani M, Kumar VG (2018) Applications of green synthesized Ag, ZnO and Ag/ZnO nanoparticles for making clinical antimicrobial wound-healing bandages. Sustain Chem Pharm 10:9–15

20. Miri A, Darroudi M, Entezari R, Sarani M (2018) Biosynthesis of gold nanoparticles using Prosopis farcta extract and its in vitro toxicity on colon cancer cells. Res Chem Intermed 44(5):3169–3177

21. Daraei A, Daraei ME (2017) Thin cylindrical slot in an optical microdisk cavity for sensing biomaterials. Applied Physics A 123:216

22. Rajesh S, Koshi E, Koshi P, Mohan A (2011) Antimicrobial photodynamic therapy: an overview. J Indian Soc Periodontol 15(4):323–327

23. Mohammadi Z, Sazgarnia A, Rajabi O, Toosi MS (2017) Comparative study of X-ray treatment and photodynamic therapy by using 5-aminolevulinic acid conjugated gold nanoparticles in a melanoma cell line. Artif Cells Nanomed Biotechnol 45(3):467–473

24. Ishi-i T, Taguri Y, Kato S, Shigeiwa M, Gorohmaru H, Maedad S, Matakab S (2007) Singlet oxygen generation by two-photon excitation of porphyrin derivatives having two-photon-absorbing benzothiadiazole chromophores. J Mater Chem 17:3341–3346

25. Arnbjerg J, Johnsen M, Frederiksen PK, Braslavsky SE, Ogilby PR (2006) Two-photon photosensitized production of singlet oxygen: optical and Optoacoustic characterization of absolute two-photon absorption cross sections for standard sensitizers in different solvents. J Phys Chem A 110(23):7375–7385

26. Zhang Y, Ha Z, Zou Q, Xing R, Jiao T, Yan X (2018) An injectable dipeptide-fullerene Supramolecular hydrogel for photodynamic antibacterial therapy. J Mater Chem B 6:7335–7342

27. Stott K, Stonehouse J, Keeler J, Hwang TL, Shaka AJ (1995) Excitation sculpting in high-resolution nuclear magnetic resonance spectroscopy: application to selective NOE experiments. J Am Chem Soc 117:4199–4200

28. Dalvit C, Bovermann G (1995) Pulsed field gradient one-dimensional NMR selective ROE and TOCSY experiments. Magn Reson Chem 33:156–159

29. Castañar L, Nolis P, Virgili A, Parella T (2014) Measurement of T1/T2 relaxation times in overlapped regions from homodecoupled 1H singlet signals. J Magn Reson 244:30–35

30. McKenna JM, Pakinson JA (2015) HOBS methods for enhancing resolution and sensitivity in small DNA oligonucleotide NMR studies. Magn Reson Chem 53(4):249–255

31. Majles Ara MH, Mousavi SH, Koushki E, Salmani S, Gharibi A, Ghanadzadeh A (2008) Nonlinear optical responses of Sudan IV doped liquid crystal by z-scan and moiré deflectometry techniques. J Mol Liq 142:29–31

32. Jafari A, Naderali R, Motiei H (2017) The effect of doping acid on the third-order nonlinearity of carboxymethyl cellulose by the Z-scan technique. Opt Mater 64:345–350

33. Dalir N, Javadian S, Dehghani Z (2017) High optical nonlinearity of nematic liquid crystal doped with graphen oxide. J Mol Liq 244:103–109

34. Sendhil K, Vijayan C, Kothiyal MP (2006) Low-threshold optical power limiting of cw laser illumination based on nonlinear refraction in zinc tetraphenyl porphyrin. Opt Laser Technol 38:512–515

35. Han P, Wang D, Gao H, Zhang J, Xing Y, Yang Z, Cao H, He W (2018) Third-order nonlinear optical properties of cyanine dyes with click chemistry modification. Dyes Pigments 149:8–15

36. He T, Cheng Y, Du Y, Mo Y (2007) Z-scan determination of third-order nonlinear optical nonlinearity of three azobenzenes doped polymer films. Opt Commun 275:240–244

37. Kityk IV, Guignard M, Nazabal V, Zhang XH, Troles J, Smektala F, Sahraoui B, Boudebs G (2007) Manifestation of electron–phonon interactions in IR-induced second harmonic generation in a sulphide glass-ceramic with b-GeS2 microcrystallites. Physica B 391:222–227

38. Jiang T, Miao R, Zhao J, Xu Z, Zhou T, Wei K, You J, Zheng X, Wang Z, Cheng X (2019) Electron–phonon coupling in topological insulator Bi2Se3 thin films with different substrates. Chin Opt Lett 17(2):020005

39. Wei K, Jiang T, Xu Z, Zhou J, You J, Tang Y, Li H, Chen R, Zheng X, Wang S, Yin K, Wang Z, Wang J, Cheng X (2018) Ultrafast carrier transfer promoted by interlayer coulomb coupling in 2D/3D Perovskite Heterostructures. Laser Photonics Rev 12(10):1800128

40. Migalska-Zalas A, EL Korchi K, Chtouki T (2018) Enhanced nonlinear optical properties due to electronic delocalization in conjugated benzodifuran derivatives. Optical and Quantum Electronics 50:389. https://doi.org/10.1007/s11082-018-1659-x

41. Lippitsch ME, Draxler S, Koller E (1992) Enhancement of the second-order hyperpolarizability of a stilbene dye by molecular interactions. Thin Solid Films 217(161):166

42. Zidana MD, Arfanb A, Allahham A (2017) Nonlinear optical investigations of quinine and Quinotoxine salts by Z-scan technique. Opt Laser Technol 89:137–142

43. Suzuki M, Yo S (1979) Inclusion compound of Cyclodextrin and Azo dye. I Methyl Orange 27(3):609–619

44. Binks DA, Spencer N, Wilkie J, Britton MM (2010) Magnetic resonance studies of a redox probe in a reverse sodium Bis(2-ethylhexyl)sulfosuccinate/octane/water microemulsion. J Phys Chem B 114:12558–12564

45. Galiullina LF, Musabirova GS, Latfullin IA, Aganov AV, Klochkov VV (2018) Spatial structure of atorvastatin and its complex with model membrane in solution studied by NMR and theoretical calculations. J Mol Struct 1167:69–77

46. Galiullina LF, Blokhin DS, Aganov AV, Klochkov VV (2012) Investigation of cholesterol model of biological membrane complex by NMR spectroscopy. MRSej 14(2):12204–12210

47. Reeves RL, Kaiser RS, Maggio MS, Sylvestre EA, Lawton WH (1973) Analysis of the visual Spectrum of methyl Orange in solvents and in hydrophobic binding sites. Can J Chem 51(4):628–635

48. Galiullina LF, Aganova OV, Latfullin IA, Musabirova GS, Aganov AV, Klochkov VV (2017) Interaction of different statins with model membranes by NMR data. BBA Biomembranes 1859:295–300